Climate network approach reveals the modes of CO 2 concentration to surface air temperature

Article *in* Chaos (Woodbury, N.Y.) · February 2021

DOI: 10.1063/5.0040360

3 authors:

Na Ying
Chinese Research Academy of Environmental Sciences
26 PUBLICATIONS **132** CITATIONS
SEE PROFILE

Jingfang Fan
Potsdam Institute for Climate Impact Research
67 PUBLICATIONS **530** CITATIONS
SEE PROFILE

Weiping Wang
Beijing Normal University
26 PUBLICATIONS **227** CITATIONS
SEE PROFILE

Climate network approach reveals the modes of CO_2 concentration to surface air temperature

Cite as: Chaos **31**, 031104 (2021); https://doi.org/10.1063/5.0040360
Submitted: 12 December 2020 . Accepted: 15 February 2021 . Published Online: 03 March 2021

Na Ying, Weiping Wang, Jingfang Fan, Dong Zhou, Zhangang Han, Qinghua Chen, Qian Ye, and Zhigang Xue

Climate network approach reveals the modes of CO_2 concentration to surface air temperature

Cite as: Chaos **31**, 031104 (2021); doi: 10.1063/5.0040360
Submitted: 12 December 2020 · Accepted: 15 February 2021 ·
Published Online: 3 March 2021

Na Ying,[1] Weiping Wang,[2] Jingfang Fan,[3,a)] Dong Zhou,[4,5] Zhangang Han,[3,a)] Qinghua Chen,[3] Qian Ye,[6] and Zhigang Xue[1]

AFFILIATIONS

[1]China State Key Laboratory of Environmental Criteria and Risk Assessment, Chinese Research Academy of Environmental Sciences, Beijing 100012, China
[2]Institute of Transportation Systems Science and Engineering, Beijing Jiaotong University, Beijing 100044, China
[3]School of Systems Science, Beijing Normal University, Beijing 100875, China
[4]School of Reliability and Systems Engineering, Beihang University, Beijing 100191, China
[5]National Key Laboratory of Science and Technology on Reliability and Environmental Engineering, Beijing 100191, China
[6]Faculty of Geographical Science, Beijing Normal University, Beijing 100875, China

[a)]**Authors to whom correspondence should be addressed:** jingfang@bnu.edu.cn and zhan@bnu.edu.cn

ABSTRACT

Increasing atmospheric carbon dioxide (CO_2) is expected to be the main factor of global warming. The relation between CO_2 concentrations and surface air temperature (SAT) has been found related to Rossby waves based on a multi-layer complex network approach. However, the significant relations between CO_2 and SAT occur in the South Hemisphere that is not that much influenced by human activities may offer not enough information to formulate targeted carbon reduction policies. Here, we address it by removing the effects of the Rossby waves to reconstruct CO_2 concentrations and SAT multi-layer complex network. We uncover that the CO_2 concentrations are strongly associated with the surrounding SAT regions. The influential regions of CO_2 on SAT occur over eastern Asia, West Asia, North Africa, the coast of North American, and Western Europe. It is shown that CO_2 over Siberia in phase with the SAT variability in eastern East Asia. Indeed, CO_2 concentration variability is causing effects on the recent warming of SAT in some middle latitude regions. Furthermore, sensitive parameters that CO_2 impacts SAT of top 15 carbon emissions countries have been identified. These countries are significantly responsible for global warming, giving implications for carbon emissions reductions. The methodology and results presented here not only facilitate further research in regions of increased sensitivity to the warming resulting from CO_2 concentrations but also can formulate strategies and countermeasures for carbon emission and carbon reduction.

The rising of atmospheric carbon dioxide (CO_2) has a great influence on global warming. The relation between CO_2 concentrations and surface air temperature (SAT) has been found related to Rossby waves. However, their dynamic modes have still remained a challenging problem, in particular for the North Hemisphere that is much influenced by human activities. In the present work, we develop a multi-layer climate network-based framework. By eliminating Rossby waves, we find that CO_2 concentrations are related to their surrounding SAT in 2 days. CO_2 concentrations variability is causing effects on the recent warming of SAT in some middle latitude regions. In addition, the critical and sensitive regions of CO_2 concentrations on SAT are identified. Our method and results presented here not only provide a deep understanding of the modes of CO_2 concentration to SAT but also can be applied to study other climate and environmental phenomena, such as global warming and air pollution.

I. INTRODUCTION

Carbon dioxide (CO_2) is one of the most important anthropogenic greenhouse gases in Earth's atmosphere. Despite global efforts to reduce CO_2 emissions, atmospheric CO_2 concentrations have been increasing worldwide since the industrial revolution reached 146% of the preindustrial level in 2017.[1] In the short term, CO_2 concentrations are widely considered to affect the weather by

influencing SAT and sea ice cover, which are key leading indicators of the annual and decadal atmospheric circulation, and, consequently, resulting in torrential rains, blizzards, drought, and other types of extreme events.[2–5] In the long term, increases in atmospheric CO_2 concentrations are believed to be the primary cause of global warming.[6] Global warming has been linked to extreme weather and climate events that have profoundly affected human societies and natural ecosystems. In addition, the impact of CO_2 concentrations on SAT should be well understood to retard the adverse impact of climate warming.

Considerable research has been devoted to assessing the relationship between CO_2 concentrations and SAT. The earliest study can be traced back to Fourier who demonstrated the atmosphere absorbs longwave radiation from the Earth's surface.[7,8] By visually inspect ice-core CO_2 measurements and reconstructed paleoclimatic records, the study found that atmospheric CO_2 has a close correlation with SAT.[9] Strong coupling relations between CO_2 and SAT derived from ice-core records at least the last 650 000 years.[10,11] However, Antarctic ice cores were not applicable for globally averaged temperature. Antarctic temperature increase led the CO_2 increase during the last deglaciation but global temperature lagged CO_2.[12] Furthermore, their relation can be estimated from observations of atmospheric CO_2 and SAT. Based on Mauna Loa and South Pole Stations, global average CO_2 concentrations lagged 4 months to the tropical mean SAT since 1960.[13] Wang *et al.* exhibited interannual variations of the CO_2 growth rate are correlated tightly with tropical land SAT during 1959–2011.[14] Humlum *et al.* found that atmospheric global mean CO_2 concentrations lag the global average SAT during 1980–2012.[15] Richardson pointed out that the conclusion violates conservation of mass[16] and temperature changes lagged 9 months in atmospheric CO_2. More recent research demonstrated that global SAT lags or leads atmospheric CO_2 depending on the type of radiative forcing as well as its time scale.[17] These previous studies suggest that there exists a strong correlation between CO_2 concentrations and SAT, however, the lead–lag role is still no complete consensus. In addition, their relationship is also calculated using climate sensitivity, which is a straightforward and efficient metric to quantify global SAT response to increasing atmospheric CO_2. Past studies suggested that the global SAT change is nearly proportional to cumulative CO_2 emissions based on the Earth system model.[18,19] However, model results are prone to uncertainties induced by different representations of carbon cycle processes in the simulations. The above studies do not provide a mechanistic understanding of how global CO_2 variability causes the change of SAT.

CO_2 retrievals from satellite measurements have found that atmospheric CO_2 concentrations are spatially unevenly distributed. However, the role of non-dynamics CO_2 to SAT was still not well understood since previous studies analyzed the role of average CO_2 on SAT instead of non-dynamics CO_2. Therefore, an improved understanding of the role of CO_2 concentrations in SAT is needed, which is beneficial to reduce CO_2 emissions through regulation and incentives.

In recent years, network theory has been found useful for better understanding spatiotemporal behavior in the climate system.[20–22] Climate networks establish correlations among climate anomalies in distant parts of the world and attempts to explain them using relevant physical phenomena. In a climate network, geography data are transformed into nodes and edges of a network that can represent spatiotemporal relationships. Nodes refer to geographical locations or grid sites, and edges are constructed based on similarities (such as cross correlations) in the variability over time between pairs of nodes. Various climate data records (such as temperature, pressure, winds, and precipitation) can be used to construct a climate network. The climate network approach can provide a powerful framework to better understanding the structure and pattern of climate phenomena such as El Niño,[23–27] North Atlantic Oscillation,[28,29] monsoon,[30] extreme rain events,[31–33] and air pollution.[34] Climate network approach has been successfully applied to SAT records and CO_2 data. For instance, based on the SAT records, Wang *et al.* studied the positive and negative correlations (links) of SAT network and identified the characteristics of Rossby waves.[35] Zhou *et al.* studied the global behavior of the climate system and captured the dominant teleconnections paths.[36] Based on CO_2, propagation links of teleconnections in CO_2 concentrations were identified.[37] In this case, climate networks provide a well-suited general framework to analyze the spatial characteristics of time series and the correlations between nodes.

The basic idea behind climate networks is that relevant and important features of atmospheric mechanisms influence the variability of CO_2 concentrations and SAT at different locations, and these influences are encoded in the structure of the network. By extracting the topological index of the network, we can reveal the underlying interaction between CO_2 concentrations and SAT. In a recent study, a multi-layer and multi-variable network analysis have been developed and applied to investigate the relations between CO_2 concentrations and SAT.[38] They documented that the function of Rossby waves for the modulation of relations between CO_2 concentrations and SAT. It showed that the connections between CO_2 concentrations and SAT are dominant in the Southern Hemisphere (SH) relative to the Northern Hemisphere (NH). More specifically, these links yield a dense stripe in a band centered at around 50°S. Note that CO_2 concentrations are mainly concentrated in the NH where the industry is developed and human activities are intensive and recent warming is more pronounced in the NH. Attention to the responsibilities of CO_2 changes on SAT in the NH could be more fundamental in curbing greenhouse gas emissions and limit adverse impacts. In this paper, we attempt to develop a framework to eliminate the influence of Rossby waves signal to identify the key area of CO_2 concentrations directly related to SAT. The multi-layer network between CO_2 concentrations and SAT is reconstructed based on the climate network approach. Furthermore, sensitive parameters that CO_2 impacts SAT of top 15 carbon emissions country has been identified to give implications for carbon emissions reductions. Our results can help to formulate strategies and countermeasures for carbon emission and carbon reduction.

II. DATA

A. Mid-tropospheric CO_2 concentrations

Atmospheric Infrared Sounder (AIRS) is the first in the new generation of high spectral resolution infrared sounder instruments flown aboard the National Aeronautics and Space Administration

(NASA) Aqua satellite mission. It is mounted on the sun-synchronous, near-polar orbiting satellite where the range of wave numbers 690–725 cm^{-1} are chosen for the retrievals of CO_2 mixing ratio in the mid-troposphere. The weighting functions of AIRS CO_2 channels peak between 300 and 500 hPa, and the CO_2 data are retrieved globally under clear and cloudy conditions. Here, we employ CO_2 concentrations measurements from AIRS with daily temporal and 2.5° × 2.0° spatial resolutions over 60°S to 80°N.[39] To keep consistent with SAT data, 100 944 nodes of CO_2 concentrations have been interpolated onto 2.5° × 2.5°. Before 2012, the AIRS retrievals are combined with the Advanced Microwave Sounding Unit (AMSU); after 2012, AIRS retrievals only applied infrared measurements because of the degradation of AMSU. To get a longer CO_2 record, we have used AIRS/AMSU retrievals and AIRS retrievals of CO_2 together in this study. The missing values from 2003 to 2016 in the CO_2 concentration grid points are removed, resulting in 322 days per year. Hence, the total time length is 4508 days.

B. SAT

SAT data obtained from the National Centres for Environmental Prediction/National Centre for Atmospheric Research (NCEP/NCAR) on daily temporal and 2.5° × 2.5° spatial resolutions are used in this study.[40] To be consistent with the length of CO_2 records, we pick 322 days in each year from 2003 to 2016 according to the date of CO_2. To keep an approximate homogeneity covering the globe (60° S–80° N), we consider a subset of N = 658 nodes of the mid-tropospheric CO_2 and SAT (see all the dots in Fig. 3). Ultimately, we obtained 658 time series and M = 432 964 pairs representing possible links.

III. METHODS

A. Data pre-processing

Linear tendency and seasonal cycle are dominant in AIRS CO_2 concentrations and SAT data. Given a CO_2 record, $\tilde{C}_i'(t)$, where i is the node index of the CO_2 concentrations ($i = 1,2,\ldots,658$) and t is the length of the CO_2 time series($t = 1,2,\ldots, 322 \times 14$). The linear trend is removed as $\tilde{C}_i(t) = \tilde{C}_i'(t) - (a_i t + b_i)$, where $a_i t + b_i$ is the linear trend of the CO_2 concentrations on the total number of day t. Leap days are excluded for simplicity. Next, we remove the long-term mean and divide by its corresponding standard deviation as $C_i^y(d) = (\tilde{C}_i^y(d) - \sum_y \tilde{C}_i^y(d)/N)/std(\tilde{C}_i^y(d))$. The effects of autocorrelations in the records are eliminated by the denominator. Finally, the anomalies CO_2 time series of each node i is rewritten as $C_i(t)$. For SAT records, $\tilde{T}_j(t)$ ($j = 1,2,\ldots,658$), we constructed their anomalies SAT as the way of CO_2 records and denoted as $T_i(t)$. After that, we get the CO_2 anomaly records $C_i(t)$ and SAT anomaly records $T_j(t)$.

B. Method of removing Rossby waves

Rossby waves corresponding weather change cycle is approximately a week (see Fig. S1 in the supplementary material). The time delay associated with the wavelengths of Rossby waves in the CO_2 concentrations and SAT multi-layer network is 3–5 days.[38] Here, moving average methods are used to removing the role of Rossby waves. We choose 7 days as an appropriate width of the window, which is explained later. We calculate a 7-day moving average for each node and then glue each 7th day in the period of the records to yield new records. We measure the correlation coefficient and link's weights based on the new glued records. Here, we explain why we choose 7 days as the width of the window. We generate new records by using the width of window range from 3 to 10 days and then calculate their positive and negative links, respectively (see Fig. S2 in the supplementary material). It is overserved that after 6 days, positive and negative link weights do not enhance around the wavelength of Rossby waves. Thus, any size of the sliding window longer than 6 days gives the results eliminating the effect of Rossby waves. Yet, the weight links yield stronger strength when using a sliding window of 7 days. Therefore, our choice of sliding window, 7 days, is suitable for evaluating the characteristic of the network.

C. Network construction

Similar to earlier studies,[34,38] we define $X_{C_i,T_j}(\tau)$ as the time-delayed cross -correlation function for the CO_2 node i and SAT node j. The time lags τ is in the range between −100 and +100 days. The time lag is chosen to be long enough to avoid the sensitive of correlation estimation to our choice of time lag, which leads to erroneous correlation estimation. The strength of the positive and negative link weights is denoted as $W^{pos}_{C_i,T_j}$ and $W^{neg}_{C_i,T_j}$. We define $\tau^{pos}_{C_i,T_j}$ and $\tau^{neg}_{C_i,T_j}$ as the corresponding time lags at these two peaks. When $\tau_{C_i,T_j} > 0$, the links are outgoing from CO_2 nodes pointing to SAT nodes; when $\tau_{C_i,T_j} < 0$, the links are pointing away from SAT nodes incoming to CO_2 nodes. Here, links with zero-time lags are excluded. The adjacency matrix of a climate network is defined as follows:

$$A^{pos}_{C_i,T_j} = \begin{cases} 1 & \text{if } W^{pos}_{C_i,T_j} \geq Q \text{ and } \tau^{pos}_{C_i,T_j} > 0, \\ 0 & \text{else,} \end{cases} \quad (1)$$

$$A^{neg}_{C_i,T_j} = \begin{cases} 1 & \text{if } W^{neg}_{C_i,T_j} \leq -Q \text{ and } \tau^{neg}_{C_i,T_j} > 0, \\ 0 & \text{else.} \end{cases} \quad (2)$$

Here, Q is a threshold for the weight links, which is determined based on the shuffling procedure.[41,42] In the shuffled case, the order of years is permutated and the order of days within each year is maintained for each pair of CO_2 and SAT nodes i and j.[41] This shuffling keeps all the statistical quantities of the original data but omits the physical dependencies between CO_2 and SAT nodes. In such a case, the shuffled network represents the properties of statistical quantities and the autocorrelations of the original records, which may introduce unrealistic links. If the original link weights are significantly higher than that of the control, we regard it as a real link; otherwise, they are spurious links. Then, we obtain the desired connection between CO_2 and SAT based on the adjacency matrix $A^{pos}_{C_i,T_j}$ and $A^{neg}_{C_i,T_j}$.

The degree is the most common application for measuring climate networks. A link that points toward a node is referred to as an in-degree link, and a link that points away from a node is considered as an out-degree link. The way of CO_2 dynamically influenced SAT is defined as the weighted out-degree of CO_2 nodes, which are the

total outgoing link weights from CO_2 nodes,[26]

$$O^{pos}_{C_i} = \sum_j A^{pos}_{C_i,T_j} W^{pos}_{C_i,T_j}, \quad (3)$$

$$O^{neg}_{C_i} = \sum_j A^{neg}_{C_i,T_j} W^{neg}_{C_i,T_j}. \quad (4)$$

And, the response of SAT to CO_2 is denoted as weighted in-degree of SAT nodes, which are the total incoming links weights pointing toward SAT nodes,

$$I^{pos}_{T_j} = \sum_i A^{pos}_{C_i,T_j} W^{pos}_{C_i,T_j}, \quad (5)$$

$$O^{neg}_{T_j} = \sum_i A^{neg}_{C_i,T_j} W^{neg}_{C_i,T_j}. \quad (6)$$

Obviously, the outgoing links of the CO_2 are the same as the incoming links of the SAT. Nodes that have higher values represent a larger amount of connection with other nodes in the network, while lower ones mean "isolated" in the network. The in and out fields describe the level of CO_2 nodes impact on the SAT nodes and the level of affected SAT node from CO_2 nodes, respectively.

D. Significance tests

The statistical significance of link weights is determined based on a shuffling procedure. In the shuffled case, the order of years is

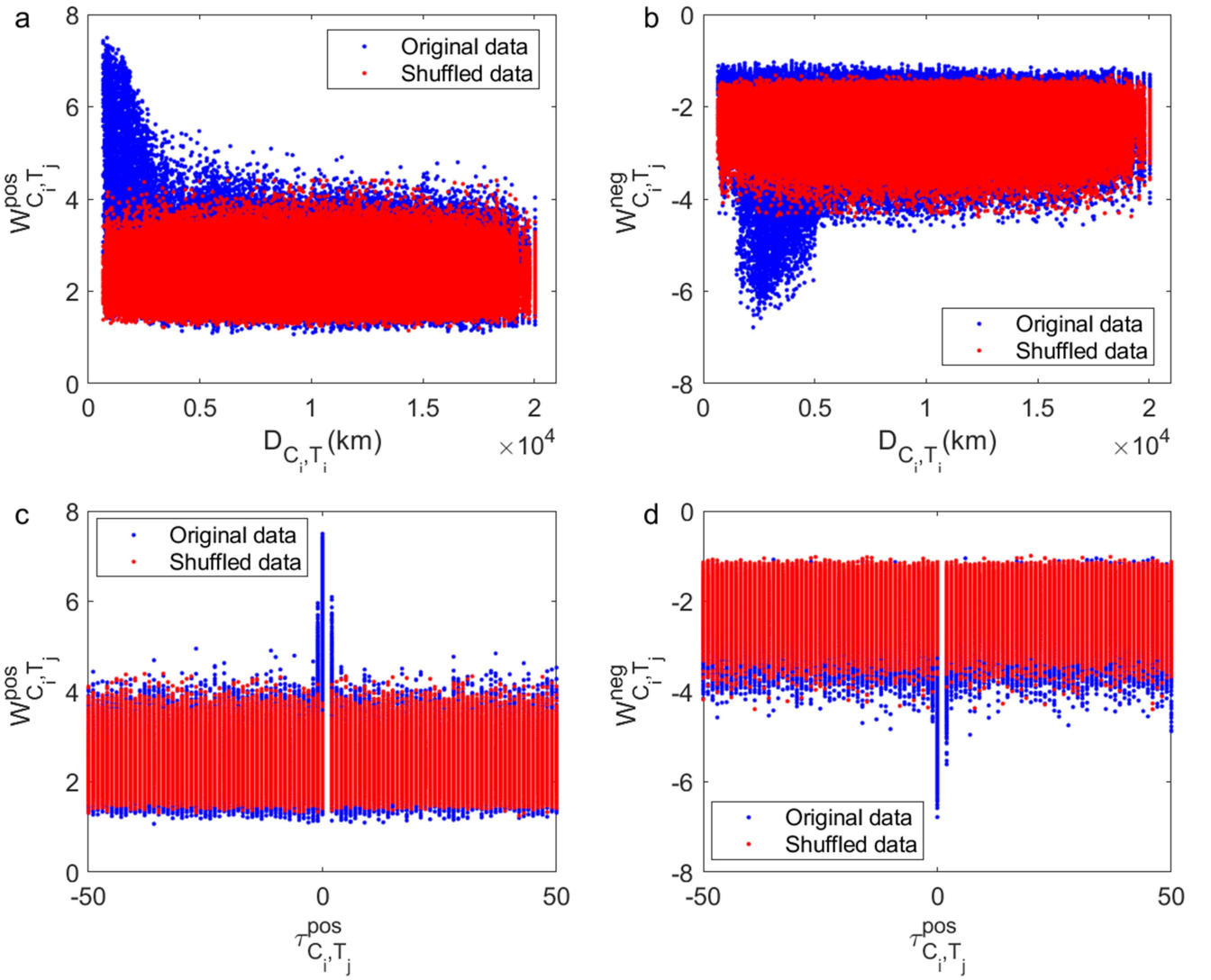

FIG. 1. (a) The positive weighted links vs their distance for both original (blue dots) and shuffled (red dots) data. (b) Same as (a) but for negative weighted links. (c) The positive weighted links vs their time lags for both original and shuffled data. (d) Same as (c) but for negative weighted links.

permutated and the order of days within each year is maintained for each pair of CO_2 and SAT nodes i and j.[41] We generate shuffled data according to the procedures described in Sec. III D. This shuffling keeps all the statistical quantities of the original data but omits the physical dependencies between CO_2 and SAT nodes. In such a case, the shuffled network represents the properties of statistical quantities and the autocorrelations of the original records, which may introduce unrealistic links. We choose a control for the records to distinguish realistic links from unrealistic ones. If the original link weights are significantly higher than that of the control, we regard it as a real link; otherwise, they are spurious links.

IV. RESULTS AND DISCUSSION

We present the main results of the correlated multi-layered networks composed of the mid-troposphere CO_2 concentrations and SAT as described above. Figures 1(a) and 1(b) display link weights (both positive and negative), W_{C_i,T_j} as a function of the geographical distances, D_{C_i,T_j} (in km) for original and shuffle cases. Higher $W^{pos}_{C_i,T_j}$ and $W^{neg}_{C_i,T_j}$ over short distances (smaller than 5000 km) are observed in the original network but not in the shuffled data, indicating the relations between CO_2 and SAT are less likely to occur by chance. It is clear that there is no strong distinction between the original and shuffled link weights as a wide range of original link weights is associated with the same shuffled link weights at a distance longer than 10 000 km. Figures 1(c) and 1(d) present W_{C_i,T_j} on the time lag for the original and shuffle case. Peaks are observed around −1, 0, and 2 days for the positive and negative links in the original network. These links in the shuffled network do not change with time lag value. Strong W_{C_i,T_j} is related to short time lags (within 2 days), suggesting that the information propagation of these links is fast.

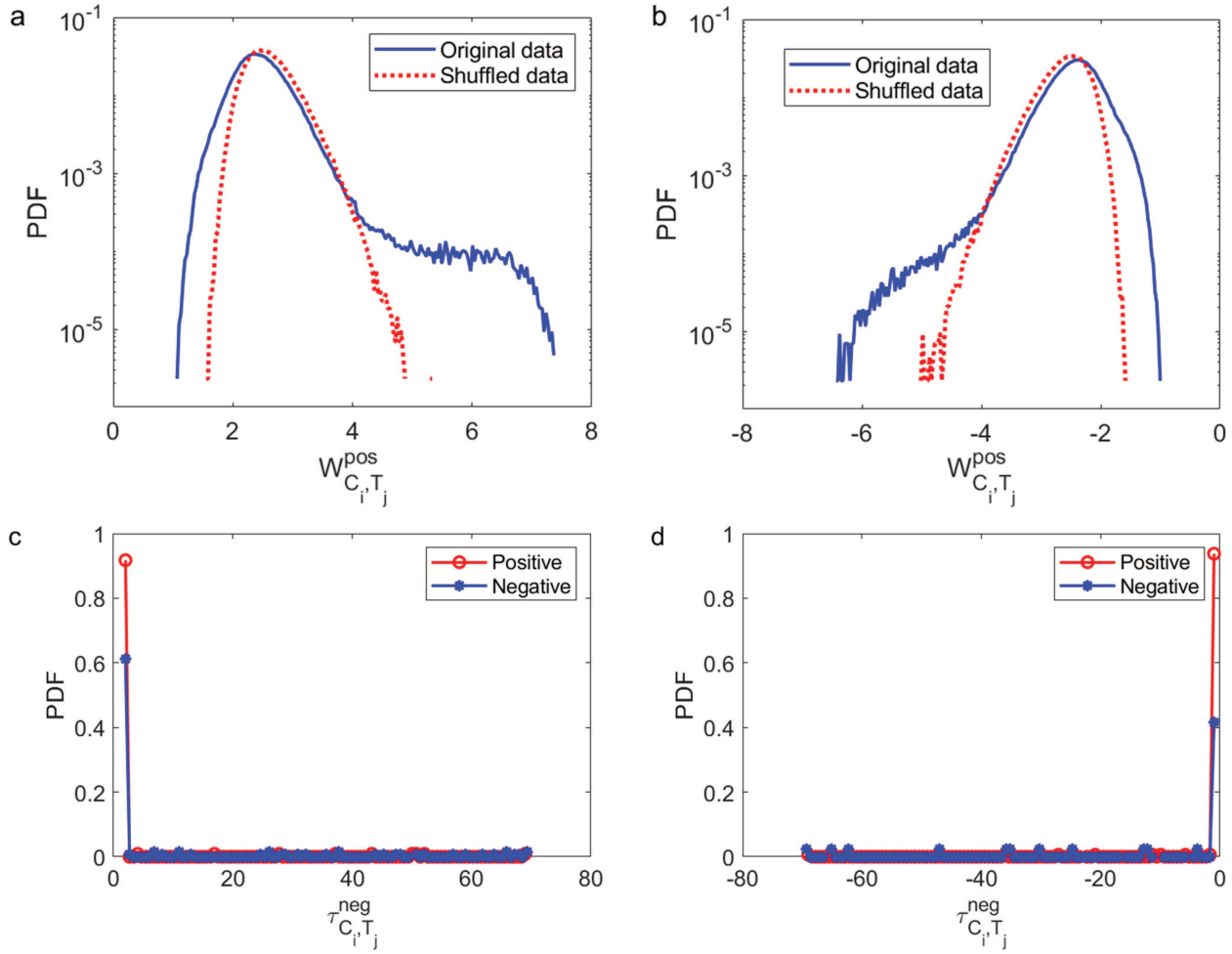

FIG. 2. (a) The PDF of the positive link weights of original (blue) and shuffled (red) data. (b) Same as (a) but for negative weighted links. (c) The PDF of time lag $\tau > 0$ of the positive and negative links. (d) Same as (c) but for $\tau < 0$.

Figures 2(a) and 2(b) show the probability density function (PDF) of $W^{pos}_{C_i,T_j}$ and $W^{neg}_{C_i,T_j}$ for original and shuffle cases. We find that values in the original network have a long tail and therefore occur due to certain physical interactions. These differences between the distribution of original data and shuffled data indicate that many significant links exist in the multi-layer network. We, thus, consider only links $|W_{C_i,T_j}| \geq 4.5$, which are separated from the shuffled links. Next, we investigate the PDF of time delays for positive and negative links. For $\tau_{C_i,T_j} > 0$ [Fig. 2(c)], the direction is toward the SAT nodes at the surface. Significant links peak with a 2-day time delay, indicating that changes in the CO_2 occur two days before the correspondingly changes in the SAT. The PDF in Fig. 2(d) shows the maximum values at −1 days, suggesting that a high CO_2 concentration is observed 1 day before a high level of SAT.

The domain CO_2 regions are quantified by the CO_2 weighted out-degrees of nodes associated with the total weights of the significant outgoing interlinks to the SAT. Figures 3(a) and 3(b) depict the map of weighted out-degrees obtained from the positive and negative links. The direction is toward the SAT nodes at the surface. We find that the most prominent positive regions are located over eastern Asia (35°–60°N, 90°–150°E), central west Asia, and southeast Canada in the Northern Hemisphere (NH). Regions in Western Asia, Western Europe, coastal areas of North America, and North parts of Africa are characteristic by clustering negative links toward SAT nodes. In the Southern Hemisphere (SH), high positive values are observed in the eastern Australia, the adjacent Pacific Ocean, and the Southern Atlantic Ocean. The negative interlinks are mainly connected to the southern South America, southern Africa and its surrounding seas, and the southern sea areas of Australia. These locations that affect the SAT are densely populated and industrialized areas.

The affected regions on the SAT are quantified by the weighted in-degrees associated with the total weights of the significant incoming interlinks from CO_2 nodes, which are presented in Figs. 3(c) and 3(d). The localized nodes of the strong positive values are found in the central-east Asia (37.5°–52.5°N, 70°–150°E) and eastern and central South America. Significant negative peaks are detectable over the eastern Asia, Western Europe, the North Atlantic Ocean, and central North America. In the SH, regions with larger positive values coincide with that of CO_2. For negative cases, the centers in a large swath of the southern Atlantic Ocean and the Indian Ocean, the south part of Africa, and Australia are highlighted. Of note is that these locations are most influenced by CO_2. If the equatorial regions are excluded, then the map of high values [Figs. 3(c) and 3(d)] to some extent resembles Fig. 3(b).[43]

Based on the weighted degree index, we further provide sensitive parameters that CO_2 impacts SAT of top 15 carbon emissions country, which is shown in Fig. 4. Four types are classified according to the weighted out-degrees. China is the world's biggest carbon emitter, as expected, it gives rise to 0.64 °C increasing per unit of ppm. In Australia, it displays an unexpected high influence value (0.43), where is not that much-emitted carbon. As the second biggest carbon emitter, the US brings to 0.32 °C increasing per unit of ppm, which is half of that in China. The values in India, Russia, Japan, and German are 0.32, 0.38, 0.35, and 0.31, respectively. The third category contains Iran, Saudi Arabia, and France, the parameters are 0.24, 0.23, and 0.3, respectively. These values in Canada, Brazil, and Korea are 0.22, 0.21, and 0.2, respectively. In summary, the rank of most weighted out-degrees is consistent with the rank of their carbon emissions. Therefore, large carbon emissions countries

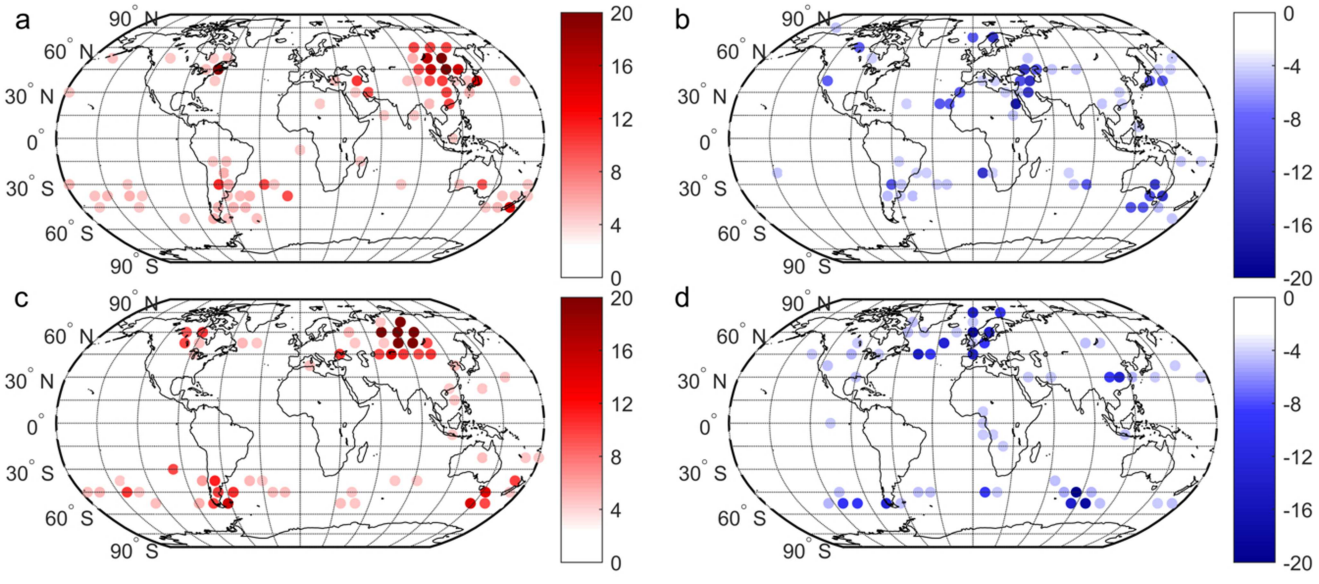

FIG. 3. The maps of weighted out-degrees (outgoing from the CO_2 nodes) for positive (a) and (b) negative links, respectively. The maps of weighted in-degrees (incoming to the SAT nodes) for positive (c) and (d) negative links, respectively.

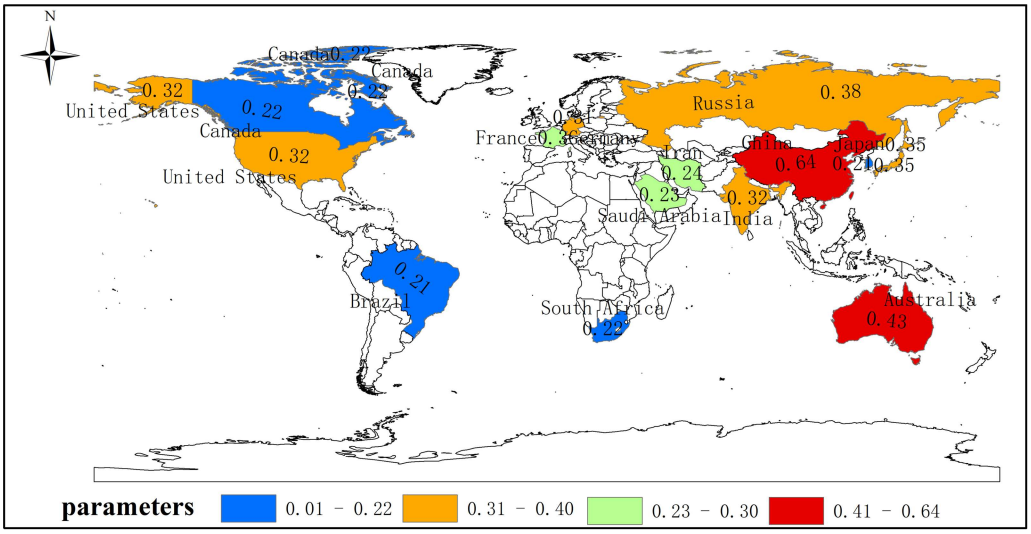

FIG. 4. Map of influence parameters of top 15 carbon emissions national.

are chiefly responsible for global warming, these countries must do more to reduce carbon emissions.

To intuitively understand the propagation process from CO_2 network to SAT network, we display their transport paths with the following characteristics: (1) the distance $\leq$7500 km and (2) $|W_{C_i,T_j}| \geq 4.5$. These 98 positive links and 31 negative links are presented in Fig. 5. We find that the links are transported from high latitude nodes to low latitude nodes. For positive links, the striking links are propagated from CO_2 in Siberia to SAT in eastern parts of East Asia, suggesting that SAT in eastern parts of East Asia is consistent with the variability of CO_2 in Siberia. These links are located over the downstream jet exit region.[44] CO_2 variability over the North Atlantic is found to be consistent with the change of SAT in the western Asia. Furthermore, the connection from CO_2 nodes over North America to the SAT nodes in eastern coastal regions is also highlight, which is a portion of wave train pattern generated by the North Atlantic Oscillation (NAO) from the North Atlantic to East Asia.[45,46] Noted that the starting point and ending point of the above links are closely associated with prominent "centers of action" over European Russia, west-central Asia, East Asia, the North Pacific, and North America.[47] To intuitively understand these propagation links, we investigated the links with Rossby waves and without Rossby waves (see Fig. S3 in the supplementary material).

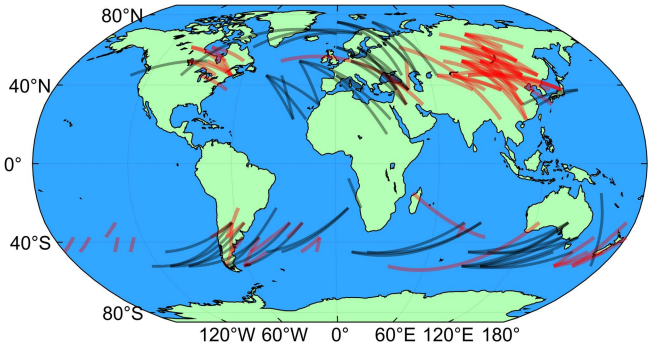

FIG. 5. The maps of propagation links for positive (red solid lines) and negative (black solid lines) links from CO_2 to SAT.

For negative cases, we observed that a group of negative links transport eastward from CO_2 in the central United States to SAT in West Europe. It indicates that changes in the CO_2 concentration are opposite to the changes in SAT. Negative links from CO_2 in North Atlantic directed to SAT in the Mediterranean region and even North Africa are also detectable. These links yield a clear connection with the North Atlantic storm track.[48] Wave trains emerging in the southern part of the North Atlantic storm track transport to the Mediterranean region and subsequently propagate eastward along with the subtropical westerly jet.[49] It is also noted that negative links propagate from CO_2 in eastern China to SAT in the Pacific Ocean, which is less pronounced. This path is probably consistent with the wave train linking Asia and North America.[50] In the SH, the connectivity pattern shows dense links in the 40°S band within the longitude from South America to Australia.

V. CONCLUSIONS

In this study, we developed a climate network approach to study the relations between CO_2 concentrations and SAT. We have found that the influence of mid-tropospheric CO_2 concentrations on SAT is significant. This is achieved by removing the Rossby waves signal in CO_2 and SAT records to construct a multi-layered network between CO_2 and SAT. The striking link weights occur in the near distance, suggesting CO_2 is strongly associated with its surrounding regions of SAT. The critical regions that CO_2 affects SAT are found to be in the eastern Asia, West Asia, eastern North American,

and Western Europe in the NH. Other successive centers of higher levels are observed in southern South America and south and east sea areas of Australia in the SH. These sensitive regions correspond to regions that are much influenced by human activities and higher CO_2 concentrations. Moreover, sensitive regions that are affected by CO_2 are observed over Siberia, Western Europe, North America, and southern South America. The influence parameters that CO_2 concentrations affected SAT of large carbon emissions country are determined. The magnitude of values, in general, conforms to the order of carbon emissions, suggesting large carbon emissions countries are chiefly responsible for global warming. In addition, explicit transport links are analyzed to investigate the process of CO_2 on SAT. The results indicate the change of CO_2 is causing effects on the recent warming of SAT in some middle latitude regions. These links follow atmosphere circulation, such as the North Atlantic storm track, NAO, and subtropical westerly jet.

Rossby waves are removed to investigate the critical regions that influence the CO_2 on the SAT and sensitive regions of SAT affected by CO_2. The identification of these regions is conducive to the development of targeted carbon reduction policies and thus mitigating the adverse effects of climate change. Our results show that recent warming in eastern East Asia may be related to the change of CO_2 concentration in Siberia. Large carbon emissions countries are chiefly responsible for global warming, which have implications for carbon emissions reductions. This study not only provides complementary support for the results from the observational data-based study and the climate modeling but also calls for attention for further research in regions of increased sensitivity to the warming resulting from CO_2. Compared with sensitive regions from the former study,[38] our results are can be more helpful for global carbon emission reduction. Moreover, our framework provides a bridge between the network analysis and the complex climate system.

SUPPLEMENTARY MATERIAL

See the supplementary material for the time lag of the function of Rossby waves in CO_2 concentrations and SAT multi-layer network and explaining the appropriate width of the window for removing Rossby waves.

ACKNOWLEDGMENTS

The participation of Dr. Na Ying in this study was supported in parts by the National Key Research and Development Program of China (Grant No. 2016YFA0602503) and the National Key Research and Development Program of China (Grant No. 2019YFC0214201). The authors wish to thank NASA for providing the AIRS mid-tropospheric CO_2 data sets and NECP for providing the SAT data sets.

DATA AVAILABILITY

The CO_2 concentration data that support the findings of this study are openly available online at https://acdisc.gesdisc.eosdis.nasa.gov/data/Aqua_AIRS_Level3/AIRX3C2D.005/ and https://acdisc.gesdisc.eosdisc.eosdis.nasa.gov/data/Aqua_AIRS_Level3/AIRX3C2D.005/. SAT data can obtained from https://psl.noaa.gov/data/gridded/data.ncep.reanalysis.surface.html, while the output data that support the findings of this study are available from the corresponding author upon reasonable request.

REFERENCES

[1]WMO 2018 Greenhouse gas bulletin No14: The state of greenhouse gases in the atmosphere.
[2]S. Schubert, D. Gutzler, H. Wang, A. Dai, T. Delworth, C. Deser, K. L. Findell, R. Fu, W. Higgens, M. Hoerling *et al.*, "A US CLIVAR project to assess and compare the responses of global climate models to drought-related SST forcing patterns: Overview and results," J. Clim. **22**(19), 5251–5272 (2009).
[3]K. L. Findell and T. L. Delworth, "Impact of common sea surface temperature anomalies on global drought and pluvial frequency," J. Clim. **23**(3), 485–503 (2010).
[4]Y. Kushnir, R. Seager, M. Ting, N. Naik, and J. Nakamura, "Mechanisms of tropical Atlantic influence on North American precipitation variability," J. Clim. **23**(21), 5610–5628 (2010).
[5]C.-P. Chang, M. Ghil, H.-C. Kuo, M. Latif, C.-H. Sui, and J. M. Wallace, "Understanding multidecadal climate changes," Bull. Am. Soc. Inf. Sci. **95**, 293–296 (2014).
[6]IPCC 2013 Working Group I contribution to the fifth assessment report of the intergovernmental panel on climate change summary for policymakers.
[7]J. B. J. Fourier, "Remarques générales sur les températures du globe terrestre et des espaces planétaires," Ann. Chim. Phys. **27**, 136–167 (1824).
[8]J. B. J. Fourier, "Mémoire sur la Température du Globe Terrestre et des Espaces Planétaires," Mémoires de l'Académie Royale des Sciences de l'Institut de France **7**, 570–604 (1827).
[9]D. C. Frank, J. Esper, and C. C. Raible, "Ensemble reconstruction constraints on the global carbon cycle sensitivity to climate," Nature **463**, 527–530 (2010).
[10]J. R. Petit, J. Jouzel, and D. Raynaud, "Climate and atmospheric history of the past 420,000 years from the Vostok ice core, Antarctica," Nature **399**, 429–436 (1999).
[11]U. Siegenthaler, T. F. Stocker, E. Monnin *et al.*, "Stable carbon cycle-climate relationship during the late Pleistocene," Science **310**, 1313–1317 (2005).
[12]J. D. Shakun, P. U. Clark, F. He, S. A. Marcott, A. C. Mix, Z. Liu, B. Otto-Bliesner, A. Schmittner, and E. Bard, "Global warming preceded by increasing carbon dioxide concentrations during the last deglaciation," Nature **484**, 49–54 (2012).
[13]J. M. Adams and G. Piovesan, "Long series relationships between global interannual CO_2 increment and climate: Evidence for stability and change in role of the tropical and boreal-temperate zones," Chemosphere **59**(11), 1595–1612 (2005).
[14]Y. Wang, A. Gozolchiani, Y. Ashkenazy, Y. Berezin, O. Guez, and S. Havlin, "Dominant imprint of Rossby waves in the climate network," Phys. Rev. Lett. **111**(13), 138501 (2013).
[15]O. Humlum, K. Stordahl, and J. E. Solheim, "The phase relation between atmospheric carbon dioxide and global temperature," Glob. Planet. Change **100**, 51–69 (2013).
[16]M. Richardson, "Comment on the phase relation between atmospheric carbon dioxide and global temperature by Humlum, Stordahl and Solheim," Glob. Planet. Change **107**, 226–228 (2013).
[17]K. E. Muryshev, A. V. Eliseev, I. I. Mokhov, and A. V. Timazhev, "Lead-lag relationships between global mean temperature and the atmospheric CO_2 content in dependence of the type and time scale of the forcing," Glob. Planet. Change **148**, 29–41 (2017).
[18]H. D. Matthews, N. P. Gillett, P. A. Stott, and K. Zickfeld, "The proportionality of global warming to cumulative carbon emissions," Nature **459**, 829–832 (2009).
[19]K. Zickfeld, A. H. MacDougall, and H. D. Matthews, "On the proportionality between global temperature change and cumulative CO_2 emissions during periods of net negative CO_2 emissions," Environ. Res. Lett. **11**(5), 055006 (2016).
[20]A. A. Tsonis, K. L. Swanson, and P. J. Roebber, "What do networks have to do with climate?," Bull. Am. Meteorol. Soc. **87**, 585–596 (2006).
[21]A. A. Tsonis, K. L. Swanson, and G. Wang, "On the role of atmospheric teleconnections in climate," J. Clim. **21**(12), 2990–3001 (2008).
[22]A. Agarwal, L. Caesar, N. Marwan, R. Maheswaran, B. Merz, and J. Kurths, "Network-based identification and characterization of teleconnections on different scales," Sci. Rep. **9**, 8808 (2019).

[23]K. Yamasaki, A. Gozolchiani, and S. Havlin, "Climate networks around the globe are significantly affected by El Nino," Phys. Rev. Lett. **100**, 228501 (2008).
[24]J. Ludescher, A. Gozolchiani, M. I. Bogachev, A. Bunde, S. Havlin, and H. J. Schellnhuber, "Improved El Nino forecasting by cooperativity detection," Proc. Natl. Acad. Sci. U.S.A. **110**(29), 11742–11745 (2013).
[25]J. Meng, J. F. Fan, J. Ludescher, A. Agarwal, X. Chen, A. Bunde, J. Kurths, and H. J. Schellnhuber, "Complexity-based approach for El Niño magnitude forecasting before the spring predictability barrier," Proc. Natl. Acad. Sci. U.S.A. **117**(1), 177–183 (2020).
[26]J. F. Fan, J. Meng, Y. Ashkenazy, S. Havlin, and H. J. Schellnhuber, "Network analysis reveals strongly localized impacts of El Niño," Proc. Natl. Acad. Sci. U.S.A. **114**(29), 7543–7548 (2017).
[27]J. F. Fan, J. Meng, Y. Ashkenazy, S. Havlin, and H. J. Schellnhuber, "Climate network percolation reveals the expansion and weakening of the tropical component under global warming," Proc. Natl. Acad. Sci. U.S.A. **115**(52), E12128–E12134 (2018).
[28]O. Guez, A. Gozolchiani, Y. Berezin, S. Brenner, and S. Havlin, "Climate network structure evolves with North Atlantic oscillation phases," Europhys. Lett. **98**(3), 38006 (2012).
[29]O. Guez, A. Gozolchiani, Y. Berezin, Y. Wang, and S. Havlin, "Global climate network evolves with North Atlantic Oscillation phases: Coupling to Southern Pacific Ocean," Europhys. Lett. **103**(6), 68006 (2013).
[30]N. Boers, B. Bookhagen, N. Marwan, J. Kurths, and J. Marengo, "Complex networks identify spatial patterns of extreme rainfall events of the South American Monsoon System," Geophys. Res. Lett. **40**(16), 4386–4392, https://doi:10.1002/grl.50681 (2013).
[31]M. Rathinasamy, A. Agarwal, B. Sivakumar, N. Marwan, and J. Kurths, "Wavelet analysis of precipitation extremes over India and teleconnections to climate indices," Stoch. Env. Res. Risk A **33**, 2053–2069 (2019).
[32]J. Kurths, A. Agarwal, R. Shukla, N. Marwan, M. Rathinasamy, L. Caesar, R. Krishnan, and B. Merz, "Unravelling the spatial diversity of Indian precipitation teleconnections via a non-linear multi-scale approach," Nonlinear Proc. Geophys. **26**(3), 251–266 (2019).
[33]N. Boers, B. Goswami, A. Rheinwalt, B. Bookhagen, B. Hoskins, and J. Kurths, "Complex networks reveal global pattern of extreme-rainfall teleconnections," Nature **566**, 373–377 (2019).
[34]Y. Zhang, J. Fan, X. Chen, Y. Ashkenazy, and S. Havlin, "Significant impact of Rossby waves on air pollution detected by network analysis," Geophys. Res. Lett. **46**(21), 12476–12485, https://doi:10.1029/2019GL084649 (2019).
[35]W. Wang, P. Ciais, R. R. Nemani, J. G. Canadell, S. Piao, S. Sitch, M. A. White, H. Hashimoto, C. Milesi, and R. B. Myneni, "Variations in atmospheric CO_2 growth rates coupled with tropical temperature," Proc. Natl. Acad. Sci. U.S.A. **110**(32), 13061–13066 (2013).
[36]D. Zhou, A. Gozolchiani, Y. Ashkenazy, and S. Havlin, "Teleconnection paths via climate network direct link detection," Phys. Rev. Lett. **115**(26), 268501 (2015).
[37]N. Ying, D. Zhou, Q. Chen, Q. Ye, and Z. Han, "Long-term link detection in the CO_2 concentration climate network," J. Clean. Prod. **208**, 1403–1408 (2019).
[38]N. Ying, D. Zhou, Z. G. Han, Q. H. Chen, Q. Ye, and Z. G. Xue, "Rossby waves detection in the CO_2 and temperature multilayer climate network," Geophys. Res. Lett. **47**(2), e2019GL086507, https:// doi:10.1029/2019GL086507 (2020).
[39]M. Chahine, C. Barnet, E. T. Olsen, L. Chen, and E. Maddy, "On the determination of atmospheric minor gases by the method of vanishing partial derivatives with application to CO_2," Geophys. Res. Lett. **32**(22), 154–164, https://doi:10.1029/2005GL024165 (2005).
[40]E. Kalnay, M. Kanamitsu, R. Kistler, W. Collins, and J. Woollen, "The NCEP/NCAR 40-year reanalysis project," Bull. Am. Meteorol. Soc. **77**, 437–472 (1996).
[41]Y. Berezin, A. Gozolchiani, O. Guez, and S. Havlin, "Stability of climate networks with time," Sci. Rep. **2**, 666 (2012).
[42]O. C. Guez, A. Gozolchiani, and S. Havlin, "Influence of autocorrelation on the topology of the climate network," Phys. Rev. E **90**(6), 29–38 (2014).
[43]A. Stips, D. Macias, C. Coughlan, E. Garcia-Gorriz, and X. S. Liang, "On the causal structure between CO_2 and global temperature," Sci. Rep. **6**, 21691 (2016).
[44]Q. Ding and B. Wang, "Circumglobal teleconnection in the northern hemisphere summer," J. Clim. **18**(17), 3483–3505 (2005).
[45]X. Zhu, O. Bothe, and K. Fraedrich, "Summer atmospheric bridging between Europe and East Asia: Influences on drought and wetness on the Tibetan Plateau," Quatern. Int. **236**, 151–157 (2011).
[46]J. Sun and H. Wang, "Changes of the connection between the summer North Atlantic Oscillation and the East Asian summer rainfall," Geophys. Res. Lett. **117**, D08110, https://doi:10.1029/2012JD017482 (2012).
[47]G. Branstator, "Circumglobal teleconnections, the jet stream waveguide, and the North Atlantic Oscillation," J. Clim. **15**(14), 1893–1910 (2012).
[48]X. Lan, P. Tans, C. Sweeney, A. Andrews, A. Jacobson, M. Crotwell *et al.*, "Gradients of column CO_2 across North America from the NOAA global greenhouse gas reference network," Atmos. Chem. Phys. **17**(24), 15151–15165 (2017).
[49]M. Sung, W. Kwon, H. Baek, K. O. Boo, G. Lim, and J.-S. Kug, "A possible impact of the North Atlantic Oscillation on the east Asian summer monsoon precipitation," Geophys. Res. Lett. **33**(21), 493–495, https://doi:10.1029/2006GL027253 (2006).
[50]J. Wang, X. Jiang, M. T. Chahine, M-C Liang, E. T. Olsen, L. L. Chen, S. J. Licata, T. S. Pagano, and Y. L. Yung, "The influence of tropospheric biennial oscillation on mid-tropospheric CO_2," Geophys. Res. Lett. **38**(20), 332–335, https://doi:10.1029/2011GL049288 (2011).